Nanoscale Chemical Analysis using Tip-Enhanced Raman Spectroscopy (TERS) and Tip-Enhanced Fluorescence (TEF)

Thomas Schmid

Department of Chemistry and Applied Biosciences,
ETH Zurich, 8093 Zurich, Switzerland

Introduction

Studying the distribution of different chemical compounds on surfaces is an important task in various fields of application, such as materials science, catalysis, and biology. The macroscale properties of materials, for example, are often affected by their structure and composition at the micro- and nanometer scale. Furthermore, a deeper understanding of biological processes can often only be achieved by a spatially resolved chemical analysis of biological interfaces, such as cell membranes and biofilms. Light microscopy techniques combined with spectroscopic methods for chemical analysis are widely used for this purpose. They provide imaging with a chemical contrast that is provided by spectroscopic measurements, work usually at atmospheric pressure and can often be operated even with the sample in a liquid environment, a prerequisite to study biological samples in their native state. Fluorescence and Raman spectroscopy are widely used for this purpose, because they provide detailed information on the chemical composition of a sample and can be coupled with a laser-scanning microscope for spatially resolved measurements. When working with conventional optics, the resolution of a microscope is limited due to optical diffraction. This contribution – after giving a short introduction to fluorescence and Raman spectroscopy – describes near-field optical methods that overcome the diffraction limit and allow fluorescence and Raman measurements with spatial resolutions in the nanometer range.

1. Fluorescence emission and Raman scattering

As schematically shown in Figure 1, fluorescence is based on the absorption of electro-magnetic radiation by a molecule (upward-pointed arrow), followed by nonradiative (wiggly line) and radiative de-excitation processes (downward-pointed straight arrow), the latter ones are summarized by the term luminescence. Luminescence emission from an excited singlet state is termed fluorescence, whereas in phosphorescence processes excited triplet states with usually much longer lifetimes are involved. According to the rule of KASHA, fluorescence emission occurs only from the lowest energy excited electronic state of an organic molecule. This rule implies that nonradiative de-excitation processes from excited vibrational states of the excited electronic state are much faster than radiative relaxation. As schematically shown in Figure 1, it is possible to excite a molecule to, for example, the $\nu' = 2$ level of the excited electronic state, but fluorescence emission only occurs from the $\nu' = 0$ level. Thus, fluorescence emission is always shifted to higher wavelengths (or lower frequencies) compared to the excitation wavelength (red shift).

Since non-radiative relaxation for most molecules is much faster than luminescence processes, most molecules do not fluoresce. Organic fluorophores are often characterized by extensive conjugated double-bond systems and condensed aromatic rings. Most of them can only be excited by UV radiation, but there are also naturally occurring (e.g. chlorophylls) or synthetic chromophores (e.g. Rhodamines) with excitation and emission in the visible spectral range. Since most molecules do not fluoresce and autofluorescence emission of biological samples is not very specific, in fluorescence microscopy the samples are most

often labeled using synthetic fluorescence markers. The labels bind specifically to the molecules of interest (analytes) and make them visible for the fluorescence microscope. Since generally fluorophores with a high quantum yield are used and the intensity of fluorescence emission is directly proportional to the intensity of excitation, modern fluorescence microscopes with laser excitation achieve high detection sensitivities, down to the single-molecule level. Thus, fluorescence microscopy can map out the distribution of certain, previously labeled molecules in a sample with very high sensitivity. This implies also the main drawback of the method: only the labeled molecules are visible. This means that staining of the sample is needed previous to the measurement, appropriate labels for the molecule of interest have to be available, and the presence of a certain analyte in the sample has to be known in advance. In other words, unexpected molecules cannot be found by fluorescence microscopy and for practical reasons, only very few different molecules can be investigated at the same time.

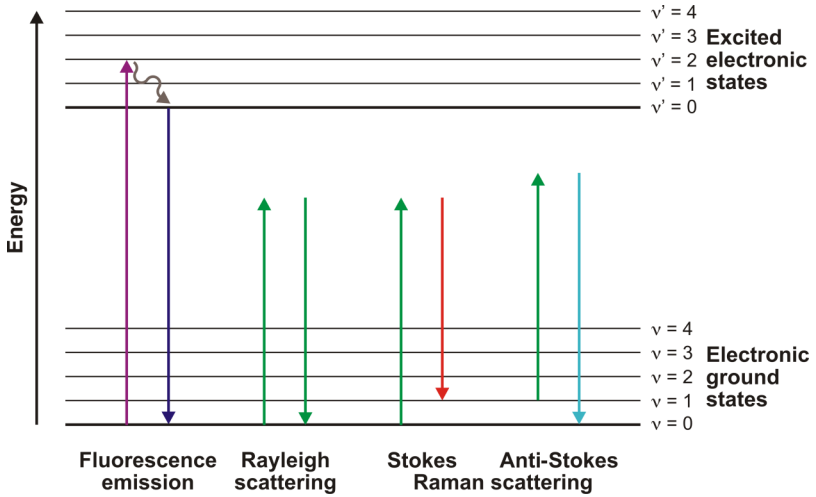

Figure 1: Explanation of fluorescence emission, Rayleigh and Raman scattering based on a Jablonski diagram.

Raman microscopy has the advantage of being a label-free technique, because most molecules can induce Raman scattering. Raman spectra are often termed as 'chemical fingerprints', because they consist of a pattern of several sharp bands that is very specific for a certain chemical structure. Functional groups, molecules and even crystal structures can be determined based on Raman spectra. The main drawback of Raman as compared to fluorescence spectroscopy is the low intensity of Raman-scattered light. Raman scattering has a cross-section that is up to 14 orders of magnitude smaller than fluorescence emission. Figure 1 explains the Raman process. As can be seen, Raman and Rayleigh denote light scattering processes that do not necessarily need a real optical absorption (including

excitation of the molecule to another electronic state) to take place. In Jablonski diagrams similar to Figure 1 scattering processes are often explained as an excitation of the molecule to 'virtual states' with a very short lifetime. These should not be misunderstood as really existing excited states. In principle, light of any arbitrary wavelength can be scattered by a molecule. Thus, the 'virtual states' can be at any arbitrary energy level. Since there is no optical absorption involved, scattering processes take place at a much shorter timescale than fluorescence. Excitation to a singlet state followed by relaxation to the ground state under fluorescence emission occurs within nanoseconds, whereas scattering processes happen at a timescale of 10^{-14}–10^{-15} seconds. Most scattered photons undergo elastic light scattering that is termed as Rayleigh scattering. Elastic light scattering means that the energy of the photon is conserved. Thus, the scattered photon has the same wavelength as the radiation employed for excitation, only its direction has changed. Only one out of approx. 10^{10} scattered photons are inelastically scattered, i.e. there is a wavelength shift between excitation light and scattered photons. The more probable effect is Stokes Raman scattering. Here, a red shift of the scattered photons is observed, because the de-excitation process ends up in an excited vibrational state. The opposite case of Anti-Stokes Raman scattering only can take place if a photon is scattered by a molecule that already was in an excited vibrational state, e.g. by thermal excitation. Since the Stokes Raman process is usually by far more probable and thus Stokes Raman bands are much more intense than Anti-Stokes, Stokes Raman is most widely used in Raman microscopy. Therefore only Stokes Raman scattering is described in this contribution. If the wavelength of the laser employed for Raman measurements coincides with an absorption band of the molecule, optical absorption will take place. Raman scattering detected after a real optical absortion is termed resonance Raman scattering (RRS). Since an excited state with a lifetime in the nanosecond range is involved, the Raman bands are of higher intensity compared to the non-resonant, normal Raman (NR) process. This resonance enhancement can increase the signal intensity by 2–3 orders of magnitude.

As can be easily seen from Figure 1, the difference in frequency of excitation and scattered photons (or the difference of the arrow lengths in Figure 1) corresponds to the frequency of a vibrational state of the molecule. The abscissa of a Raman spectrum is given by the Raman shift, which is the frequency difference between the laser light employed for excitation and the Raman scattered light. The Raman shift is expressed in wavenumbers (cm^{-1}) and corresponds to the wavenumber axis of an infrared (IR) spectrum. A molecule having an IR absorption band at a certain wavenumber often also has a Raman band at the same position, but the bands differ significantly in intensity due to different selection rules. Due to this reason OH stretching bands, for example, are very strong in IR and hamper often the analysis of samples with high water content, but are very weak in Raman spectroscopy, that is a clear advantage of Raman over IR microscopy in the study of biological systems.

2. The diffraction limit of light

As mentioned above, fluorescence and Raman spectroscopy can be coupled to microscopy for spatially resolved chemical analysis of samples. In modern fluorescence and Raman microscopes, a laser beam focused by an objective lens is scanned over a sample (or the sample is scanned through the laser focus) and fluorescence emission or Raman scattering are collected at every pixel, usually through the same objective. The lateral resolution of an optical microscope is limited due to optical diffraction. E. ABBE (1873) [1] and LORD RAYLEIGH (1879) [2] where the first to develop comprehensive theories of light diffraction and gave criteria for calculating the resolution of an optical microscope, that is the smallest distance between two resolvable microscopic objects. The RAYLEIGH criterion is given as follows [2]:

$$\Delta x = 0.61\frac{\lambda}{NA} = 0.61\frac{\lambda}{n\sin\Theta} \qquad (1)$$

Here, Δx is the lateral resolution, λ denotes the wavelength of light and NA is the numerical aperture of the objective used. The latter is given as product of the refractive index n and the sine of the half-angle Θ of the maximum cone of light that can enter or exit the objective. Air objectives by definition can reach a maximum NA of 1. Higher numerical apertures of up to 1.4–1.6 can be achieved using oil immersion objectives. As can be seen, the lateral resolution of an optical microscope depends on the wavelength of the light employed for excitation and the numerical aperture of the objective. The simplified expression of $\Delta x \approx \lambda/2$ usually gives a good estimation for the resolution that can be theoretically achieved. Thus, the best resolution that can be achieved with an optical microscope using lens optics is on the order of 400 nm / 2 = 200 nm. This contribution describes optical near-field techniques that allow to overcome the diffraction limit and gather chemical information of samples with a resolution of < 100 nm.

3. Scanning near-field optical microscopy (SNOM)

The diffraction limit is valid only in the optical far field. If a small light source is guided in very close distance over a sample (within the optical near field), the resolution of the collected microscope image does not depend on optical diffraction but is only determined by the size of the light source. In the following sections there are ideas described on how to generate very small light sources and how to scan them over a sample in distances of only a few nanometers. A historical overview on their development with a focus on fluorescence and Raman measurements is given.

3.1 Aperture SNOM

In 1928 E.H. SYNGE [3] proposed the idea to employ a small aperture for imaging surfaces with sub-wavelength resolution using visible light. An opaque metal screen with an aperture smaller than the wavelength of light (e.g. 100 nm) is illuminated from back and scanned over the sample surface (see Figure 2a). If the distance between aperture and surface is within the near-field regime (a few nanometers), the resolution of such a microscope is not limited by optical diffraction but rather defined by the size of the aperture. First experimental evidence for this idea was demonstrated by E.A. ASH and G. NICHOLLS in 1972 [4]. They reached a resolution of $\lambda/60$ using a scanning near-field microwave microscope and 3-cm radiation. Development of scanning near-field microscopes for the visible optical range became possible only after invention of the STM [5] and related techniques, which allowed controlling distances in the nanometer range between a scanning tip and a sample surface. In 1984, D.W. POHL *et al.* at IBM Zurich / Rüschlikon [6] and independently A. LEWIS *et al.* at Cornell University [7] demonstrated the first SNOM working with visible light at resolutions of approximately $\lambda/20$.

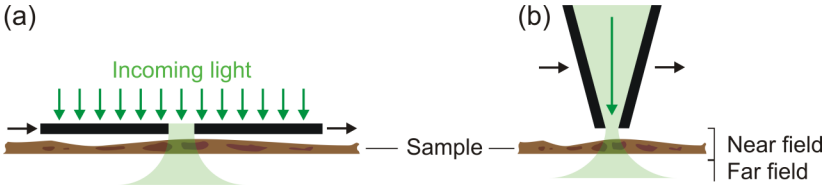

Figure 2: Synge's idea of scanning a backside-illuminated opaque metal screen with a small aperture in close distance over a sample for imaging with sub-wavelength resolution (a) compared to the principle of an aperture SNOM probe consisting of a glass fiber tip coated with an opaque metal film having a small aperture at the tip end (b).

In illumination mode SNOM, light is coupled into a fiber, which ends in a sharp tip that is scanned over the sample surface (see Figure 2b) [8]. Different feedback mechanisms are used to control the distance between probe and sample. Most often shear-force tip feedback is applied with the tip glued to a laterally oscillating piezoelectric tuning fork. When the tip is brought into close contact with the surface, the oscillation is damped due to interaction forces. The amplitude of the oscillation is monitored and is used to generate a feedback signal to control the tip-sample gap during the measurement. The tip is usually coated with an opaque metal layer, which prevents leaking of light from the side walls of the probe and provides illumination through a small (several tens to a few hundreds of nanometers diameter) aperture at the tip end. The light transmitted or reflected by the sample is collected in the far field with conventional optics. Contrary, in collection mode SNOM the sample is illuminated in the far field, and the light from an area with sub-wavelength diameter is collected by a scanning fiber probe.

In the first years after its invention, SNOM was mainly applied to luminescence and fluorescence measurements, reaching lateral resolutions of a few tens of nanometers and sensitivities in the single-molecule range. The exceedingly low Raman cross-sections of many samples as well as the small light transmission coefficients and low damage thresholds of metal-coated fiber probes hampered the development of SNOM-Raman for about 10 years. D.P. TSAI *et al.* demonstrated the collection of near-field Raman spectra for the first time in 1994 [9], and in the following years mainly the groups of BATCHELDER [10, 11] and HALLEN [12, 13] performed pioneering work in SNOM-Raman imaging. Later on, improvements in fiber probe fabrication and studies on combinations of SNOM-Raman with surface-enhanced Raman scattering (SERS) and resonance Raman scattering allowed applications of this techniques in chemistry and biology, but still the low throughput of fiber probes hampers the use of aperture-based near-field Raman imaging in many fields of application [14-16].

3.2 Apertureless SNOM

Limitations caused by the small throughput of aperture fiber probes can be overcome by using apertureless near-field methods. After the invention of the STM by G. BINNIG, H. ROHRER, C. GERBER, and E. WEIBEL at IBM Zurich / Rüschlikon in 1982 [5], J. WESSEL proposed the combination of surface-enhanced spectroscopy (Raman or second-harmonics generation) with STM in 1985 [17]. In contrast to surface-enhanced Raman scattering (SERS), where the sample is coated onto a rough metal surface that provides enhancement of the electromagnetic field and of the Raman signals, in tip-enhanced Raman spectroscopy (TERS) and tip-enhanced fluorescence (TEF) the enhancing metal structure is brought into close contact with the sample from outside by a sharp full-metal or metal-coated tip. Surface plasmons excited at the apex of the tip act as an apertureless optical probe. When the tip is scanned over the surface, Raman or fluorescence microscopy with sub-micrometer resolution becomes possible.

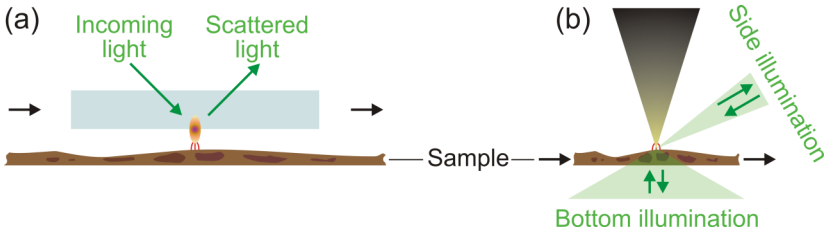

Figure 3: Wessel's idea of using a resonantly enhanced metal particle mounted on a transparent probe holder as a nanometer-sized light source (a) compared to bottom and side-illumination configurations used in TERS and TEF experiments (b). The red field lines represent the enhanced electromagnetic field at the tip end.

Interestingly, E.H. SYNGE had already a very similar idea in 1928. He proposed to use the light scattered by a small particle that is illuminated under total internal reflection from the back and scanned in close distance over the sample as excitation source for microscopy. Before publishing, SYNGE sent his ideas to A. EINSTEIN, who in a short reply told him that the basic concept seems to be reasonable but the method SYNGE proposes for its implementation, EINSTEIN found "fundamentally unusable" ("prinzipiell unbrauchbar") [18]. In a second letter, SYNGE came up with his original idea of using a small aperture in a metal screen or at the end of a quartz tip (that is very similar to aperture SNOM probes used nowadays) as a light source, and EINSTEIN encouraged him to publish his ideas in a scientific journal and to indicate the difficulties of their realization. This ended up in SYNGES publication mentioned above [3].

Light scattering by nanometer-sized structures is used nowadays for near-field investigagtions, for example in the infrared range [19-22]. WESSEL's idea was to resonantly enhance the particle and to generate a locally enhanced electromagnetic field, an effect known from SERS. The particle that is for example mounted at the end of a tip is scanned over the sample surface and allows collecting images with nanometer-scale resolution. WESSEL did not know about SYNGE's idea, but was rather inspired by the invention of the STM and discovery of SERS. In 1989 U.C. FISCHER and D.W. POHL demonstrated a first proof-of-principle of this idea by imaging a metal film with 320-nm holes with a resolution of 50 nm using a laser-illuminated polystyrene nanoparticle that was coated with a gold thin-film as apertureless SNOM probe [23]. It took 10 years more until the first spectroscopic applications of this idea were published. In 1999, E.J. SANCHEZ, L. NOVOTNY, and X.S. XIE published experimental results of tip-enhanced two-photon fluorescence measurements [24] and in 2000, the groups of R. ZENOBI [25], M.S. ANDERSON [26], and S. KAWATA [27] independently have shown tip-enhanced Raman scattering for the first time.

4. Theoretical Aspects

Electromagnetic field enhancement by a sharp full-metal or metal-coated tip can be due to different mechanisms, which in practice often occur at the same time [28]:

- Lightning rod effect
- Localized surface plasmon resonances
- Antenna resonances

Additional effects that can enhance or attenuate Raman or fluorescence signals are explained below. The lightning rod effect is a purely shape-induced effect. Geometric singularities of an irradiated metallic structure, such as a very sharp tip apex, lead to highly localized surface-charge densities that can be the source of a highly enhanced electromagnetic field. The lightning rod effect is almost independent of the excitation wavelength. If the laser wavelength coincides with a localized surface plasmon resonance of the tip, the metal will absorb part of the laser power and surface plasmon polaritons will be excited. These are collective vibrations of electrons, which can be the source of a localized

and enhanced evanescent field around the tip apex. The surface plasmon resonance wavelength depends on shape and material properties of the tip. Thus, basically there are two possibilities to optimize the surface plasmon enhancement effect: first, optimize material and shape of the tip, or second, tune the laser wavelength to efficiently overlap with an absorption band of the tip. Also the third enhancement effect is wavelength-dependent. Antenna resonances are enhanced if the length of the tip equals to multiples of half the wavelength of radiation. Also in this case, an enhanced and highly localized electromagnetic field is observed at the tip apex. As mentioned, in practice combinations of these effects occur and the enhancement factor of a tip basically depends on material properties of the tip and surrounding medium, tip size and shape as well as the laser wavelength employed.

As known from SERS theory and experiments, by far highest enhancements are achieved with aggregates of several metallic nanostructures. Small, nanometer-sized gaps between silver or gold nanoparticles, for example, can highly confine and enhance the electromagnetic signal, and in some cases, single-molecule sensitivity has been achieved with colloidal aggregates or other combined nanostructures. This effect is used in the so-called 'gap-mode' TERS configuration to achieve better light confinement and stronger signal enhancement [29]. Gap-mode TERS measurements even with single-molecule sensitivity have been shown by different groups [30-32]. The best evidence for single-molecule sensitivity was given by J. STEIDTNER and B. PETTINGER who were able to image single molecules in STM using a TERS setup that was built into a ultra-high vaccum (UHV) chamber and to collect TERS spectra with a lateral resolution of 15 nm [32]. The TERS signal intensity was directly proportional to the number of molecules in the active area of the spectroscopic measurement. In the publication images and spectra of 1 and 5 dye molecules of brilliant cresyl blue (BCB) are shown. Figure 4 shows calculated field enhancements for Au tips on a glass and a Au substrate, respectively [33]. In both cases, a highly localized and enhanced electromagnetic field can be observed at the tip apex. In the case of the gold substrate, the gap-mode effect leads to stronger confinement and field enhancements that are more than an order of magnitude larger.

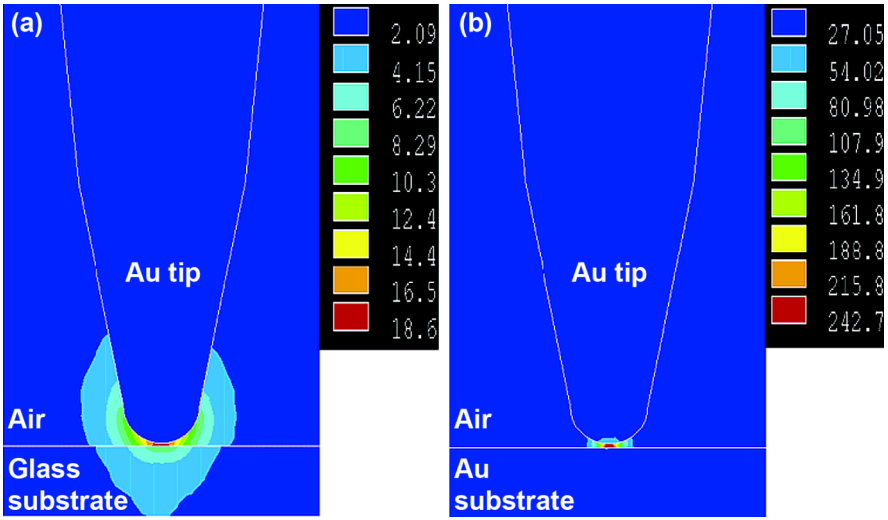

Figure 4: Calculated electromagnetic field enhancements (finite-difference time-domain method, FDTD) for laser-illuminated 20-nm radius Au tips on a glass (a) and a Au substrate (b), respectively. Adapted from Ref. [33], Copyright 2005, with permission from the American Chemical Society.

4.1 Enhancement factor and contrast

For the experimental determination of enhancement factors in TERS and TEF, two ratios have to be measured or estimated: (1) the ratio between near-field (tip-enhanced) and far-field signal intensities, and (2) the ratio between the areas or volumes, respectively, of the sizes of the far-field and near-field signal sources. Ratio (1) is termed contrast. There are two different definitions of the contrast used in the literature:

$$C = \frac{S_{tip}}{S_0} \tag{2a}$$

$$C = \frac{S_{near\ field}}{S_{far\ field}} = \frac{S_{tip} - S_0}{S_0} = \frac{S_{tip}}{S_0} - 1 \tag{2b}$$

Definition (2a) is of more practical relevance, because it is a direct measure for the image quality that can be obtained in a tip-enhanced spectroscopy experiment. Especially in the case of relatively weak enhancement, the signal S_{tip} measured with the tip engaged is superimposed with a non-enhanced background S_0 that is also obtained without a tip in close

proximity to the sample. The background signal S_0 is generated on the whole sample area or volume that is irradiated by the laser focus and therefore the presence of a strong background signal blurs the resolution of the obtained image. Definition (2b) is more precise when enhancement factors are calculated that are compared to numerical simulations or SERS measurements. This definition gives the ratio of near-field ($S_{near\ field}$) and far-field signal intensities ($S_{far\ field}$). As can be seen, both definitions differ only by a value of 1. Thus, the difference between definitions (2a) and (2b) is only significant in the case of weak enhancement.

The enhancement factor *EF* of fluorescence or Raman signals, respectively, takes into account that the sources of near-field and far-field signals are different. The near field signal is only generated in very close proximity to the tip. The diameter of the tip apex that can be determined by scanning electron microscopy (SEM) is a good estimate for the diameter of the near-field signal source. The source area of the far-field signal is given by the area of the laser focus spot. The product of contrast times the ratio of far-field ($A_{far\ field}$) and near-field source areas ($A_{near\ field}$) yields the signal enhancement factor relevant for both, TEF and TERS experiments:

$$EF = C\frac{A_{far\ field}}{A_{near\ field}} \tag{3}$$

This definition is valid for thin-film and opaque samples. If contributions to the far-field signal from bulk material are significant, far-field and near-field volumes instead of areas have to be taken into account. A more detailed description of definitions of contrast and enhancement factors including a comparison of TERS enhancement factors published in literature can be found in Ref. [34]. In practice for determining enhancement factors, signal intensities with and without the tip in contact with the sample are determined and source areas or volumes are estimated based on tip and laser focus sizes and enhancement factors are calculated according to the given definitions.

4.2 Tip-enhanced fluorescence (TEF)

The electromagnetic field enhancement factor *g* is defined as the ratio between the electromagnetic field strength at the tip E_{tip} and the electromagnetic field at the sample without a tip in contact E_0 [28, 35].

$$g = \frac{E_{tip}}{E_0} \tag{4}$$

The intensity of an optical signal depends on the sqare of the electromagnetic field strength. Thus, the enhancement factor of fluorescence intensity EF_{fluo} can be defined as the product of g^2 and the ratio of the fluorescence quantum yields with and without influence of

a tip η_{tip} / η_0. The quantum yield can be understood as the ratio of the number of fluorescence emission events over the sum of fluorescence and nonradiative relaxation events per time unit [28, 35].

$$EF_{fluo} = \left(\frac{E_{tip}(\lambda_{ex})}{E_0(\lambda_{ex})} \right)^2 \left(\frac{\eta_{tip}(\lambda_{fluo})}{\eta_0(\lambda_{fluo})} \right) = g(\lambda_{ex})^2 \left(\frac{\eta_{tip}(\lambda_{fluo})}{\eta_0(\lambda_{fluo})} \right) \qquad (5)$$

The formula contains basically two factors, which affect the fluorescence enhancement by a tip: (1) the square of the electromagnetic field enhancement at the excitation wavelength λ_{ex}, and (2) the enhancement of the fluorescence quantum yield at the wavelength of fluorescence emission λ_{fluo}. Factor (1) basically depends on properties of the tip and factor (2) depends on properties of the fluorophore. The formula implies that tip-enhanced fluorescence works best with fluorophores having low quantum yields. If molecules with high quantum yields are used, i.e. molecules having $\eta_0 \approx 1$, there is not much space for enhancement of the fluorescence emission, because the fluorescence quantum efficiency by definition has a maximum value of 1.

If a fluorophore is bound to a metal surface, the fluorescence emission can be quenched. Energy transfer from the molecule to the metal can increase the rate of nonradiative relaxation processes and thus significantly lower the fluorescence quantum yield. Quenching effects coincide with enhancement effects in tip-enhanced fluorescence experiments using full-metal or metal-coated tips. Since quenching can only take place when the molecule is in close contact with the metal, whereas field enhancement is observed up to tens of nanometers around a tip, it is mainly the tip–sample distance that determines which effect is predominant: quenching for very small distances and enhancement at distances from a few up to tens of nanometers. The superposition of fluorescence quenching and enhancement leads to an optimum tip–sample distance where the most intense fluorescence can be observed. L. NOVOTNY and co-workers have calculated this effect for the distance between a molecule and an enhancing gold nanoparticle and found very good agreement with experimental data (see Figure 5a) [36].

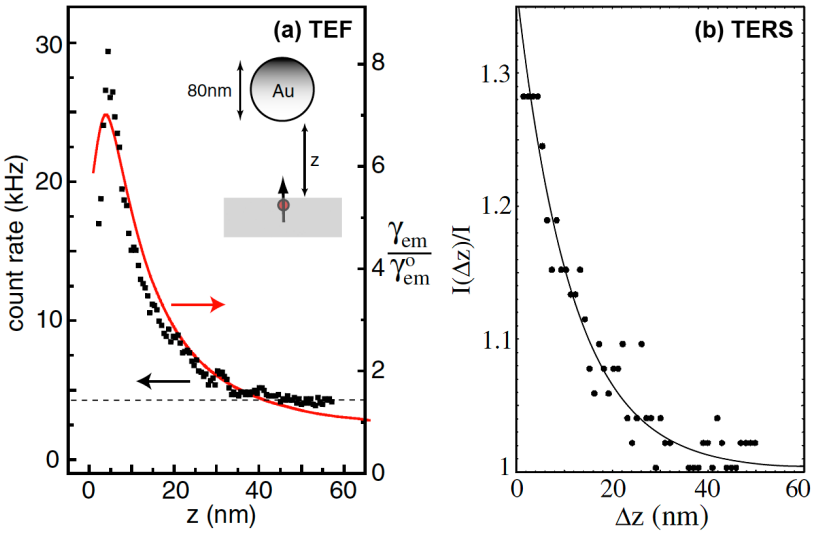

Figure 5: Dependence of the signal enhancement factor on tip-sample distance shown for TEF (a) and TERS (b). Figure 5a gives experimental (dots) and theoretically calculated data (b) for the ratio of fluorescence emission rates with and without a tip (this ratio is proportional to the enhancement factor) for different distances between a 80-nm diam. Au sphere attached to a pointed optical fiber probe. In Figure 5b, the dependence of the ratio of near-field and far-field signal intensities on the distance between a Ag tip and a single-walled carbon nanotube in a TERS experiment is shown. Figure 5a adapted from Ref. [36], Copyright 2006, with permission from the American Physical Society. Figure 5b adapted from Ref. [37], Copyright 2003, with permission from the American Physical Society.

4.3 Tip-enhanced Raman spectroscopy (TERS)

As already mentioned, TERS is very similar to SERS. In both cases, the Raman signal is dramatically enhanced by metallic nanostructures. Usually, various enhancement mechanisms occur simultaneously, which result in enhanced Raman scattering. Lightning rod effect, surface plasmon resonances, antenna resonances and gap-mode effect have already been mentioned. Similar to SERS, also in TERS chemical enhancement can additionally increase the signal intensity. If analyte molecules are in very close proximity to the enhancing metallic nanostructures, they can chemically bind to the metal via non-covalent or covalent interactions. This can lead to Raman band shifts and a selective enhancement of bands that are assigneable to the functional groups involved.

The signal enhancement factor in TERS depends on the enhancements of the light intensity at the excitation wavelength $I(\lambda_{ex})$ and of the Raman scattered light intensity $I(\lambda_{Raman})$ [28]:

$$EF_{Raman} = I(\lambda_{ex}) \cdot I(\lambda_{Raman}) = g(\lambda_{ex})^2 \cdot g(\lambda_{Raman})^2 \approx g^4 \qquad (6)$$

Since Raman shifts are often very small on the wavelength scale, i.e. $\lambda_{ex} \approx \lambda_{Raman}$, the approximation of $EF_{Raman} \approx g^4$ is sometimes found in the literature, which allows a rough estimation of the electromagnetic field enhancement g based on experimentally determined Raman enhancement factors EF_{Raman}. It should be pointed out that for an exact determination of the enhancement factor, for example for comparison with numerical simulation data, differences between the field enhancements at λ_{ex} and λ_{Raman} definitively have to be considered [38]. The enhancement is strongest in the case of close contact between tip and sample and drops dramatically with increasing tip-sample distance (see Figure 5b) [37]. Figure 5 reveals that the enhanced field at the tip extends only 10–30 nm in sample direction. Thus, TEF and TERS can be considered as techniques for surface and sub-surface analysis.

5. Experimental setups

Apart from material, size and shape of the tip, efficient illumination of the tip and collection of fluorescence or Raman signals, respectively, are crucial in TEF and TERS experiments. The optical properties of the sample determine, which of the possible setups for tip-enhanced spectroscopy can be used [34, 39]. In the case of transparent samples, illumination of the tip apex and signal collection from below is surely the most efficient optical arrangement. By using thin, transparent sample substrates, such as glass cover slips, the objective can be placed in very close distance to the sample allowing the use of oil immersion objectives with very high numerical apertures of up to 1.4–1.6. This allows tight focusing around the tip that reduces the far-field signal as well as highly efficient collection of the fluorescence emission or Raman scattering over a wide range of emission angles (see Figure 6a). Such setups are often based on home-built combinations of commercial inverted laser-scanning microscopes with a scanning probe microscope (SPM), such as AFM, STM or shear-force feedback-based SPM. Recently, some AFM producers have started collaborations with suppliers for Raman or fluorescence microscopy, and commercial SPM–Raman or SPM–fluorescence microscopy combinations have become available. Such an instrument combines the imaging and spectroscopic capabilities of a laser-scanning microscope with nanometer-scale imaging offered by SPM. Combined optical and SPM measurements at the exactly same part of a sample is advantageous for many fields of application. Imaging of the tip followed by exact positioning of the laser spot by using a laser-scanning microscope allows very precise laser–tip alignment for TEF or TERS in a relatively simple way. If besides simple ‘tip in–tip out’ experiments on single spots of the sample surface, TEF or TERS line scans or even two-dimensional mapping experiments for TEF and TERS imaging should be performed, a piezoelectrically driven sample-scanning stage is additionally

needed. In such an experiment, the laser spot is first aligned to the most enhancing site of the tip and then the sample is scanned through the laser focus while keeping the laser–tip alignment fixed.

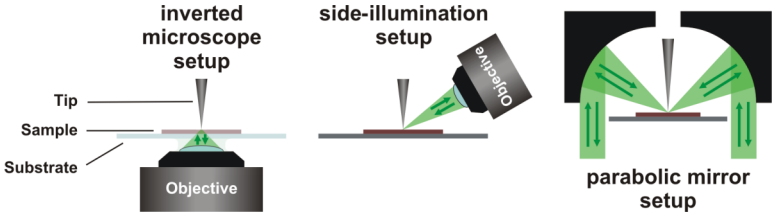

Figure 6: Simplified schemes of the most common setups for TEF and TERS: inverted microscope setup for transparent samples, side-illumination and parabolic mirror setup for opaque samples.

In the case of an opaque sample, side-illumination geometries are most often used (see Figure 6b). Here, tip illumination and signal detection are performed from the side, for example under an angle of 60°. Advantages of this configuration are the possibility to work with non-transparent samples and the use of light that is linearly polarized parallel to the tip axis, which can more efficiently excite locally enhanced fields at the tip apex. A clear drawback is the necessity to use long-working distance objectives, which have much smaller numerical apertures as in the case of Figure 6a. This leads to larger focus spots, that are asymmetric due to the side-illumination and to dramatically reduced collection efficiencies. Furthermore, the above-mentioned advantages of a laser-scanning microscope cannot be achieved in a side-illumination geometry. Parabolic mirror setups (see Figure 6c) can overcome the problems caused by the reduced focus quality by offering NAs of approximately 1 in air, having no chromatic aberrations and working even in UHV [40]. It should be pointed out that the alignment of parabolic mirrors is very delicate since small deviations from the optimum lead to substantially reduced focus qualities and collection efficiencies. A new, top-illumination configuration for non-transparent samples that is under development by our group is described in section 6.2. This setup is a combination of an upright laser-scanning microscope with AFM or STM, respectively.

5.1 Tip fabrication

There are three kinds of feedback mechanism used to keep the tip in a small and constant distance from the sample: AFM, STM, and shear-force feedback [34, 39]. In a shear-force setup with a laterally oscillating piezoelectric tuning fork, almost every kind of full-metal tip can be used for TEF or TERS, but it can be very tedious to glue the tip to the tuning fork and get a stable feedback.

AFM is surely the most versatile and most widely used member of the family of SPM techniques. It can be applied to almost every sample surface that is reasonably flat (flatness

<5–10 µm is usually required). It can be operated in different modes, such as contact and semi-contact ('tapping') mode and can yield information that is complementary to the standard topography contrast, such as phase, lateral force or magnetic force imaging. For tip-enhanced spectroscopy experiments, commercially available AFM tips are employed that are metallized by the user. Most common methods for metallization are based on physical deposition of a thin metal layer, either by vapor or sputter coating. Nominal layer thicknesses coated onto the tip are usually on the order of a few tens of nanometers. It should be pointed out that these values are usually based on measurements by a quartz crystal microbalance mounted inside the coating chamber having a horizontal and relatively large (several millimeters diam.) active area. Such a coating usually leads to a very thin layer of small metal nanoparticles at the tip apex, somehow similar to a rough SERS substrate. Since vapor and sputter coating are stochastic processes, there is only a certain probability that a strongly enhancing particle is placed exactly at the tip apex. This is one of the reasons why for every tip metallization procedure, there is only a certain fraction of tips showing enhancement in TEF or TERS experiments. More complicated approaches for AFM tip metallization and shaping, e.g. by focused ion beam (FIB) milling, can probably improve the reproducibility of TEF and TERS tip fabrication in future, but are of minor relevance nowadays. The metals used are most often silver and gold, because they can provide reasonable enhancements in the visible spectral range. Experiments with different tip materials than the most common silicon and with pre-coatings with certain dielectric materials to selectively shift the surface plasmon resonance frequency towards the laser wavelength are described in section 6.2.

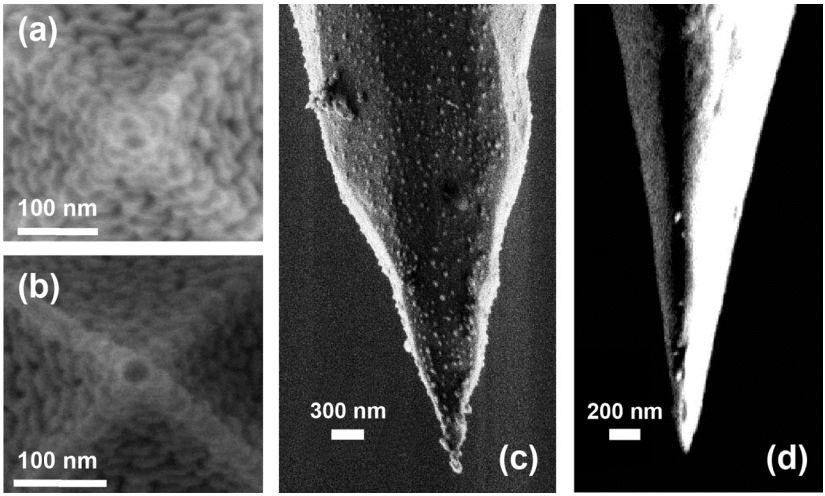

Figure 7: SEM images of TERS tips: AFM tips coated with SiO_x (a) and AlF_3 (b) followed by a layer of Ag, and STM tips prepared by electrochemical etching of Au (c) and Ag wires (d). Adapted from Ref. [39].

For tip-enhanced spectroscopy in an STM configuration, most often electrochemically etched silver or gold tips are used. In a typical etching setup, a thin silver or gold wire is one of the electrodes with a ring counter electrode around it. Both electrodes are immersed in an etching solution, which forms a meniscus at the noble metal wire. Due to this meniscus, a sharp tip is formed at the liquid–air boundary. At the end of the etching process, the lower part of the wire falls off and the current drops. Electrochemical etching allows the fabrication of symmetric and sharp full-metal tips that can be scanned over a metal surface in STM feedback. FIB milling is sometimes used for further sharpening of the tips. The fact that an STM can be operated only with conductive sample surfaces is both, drawback and advantage for tip-enhanced spectroscopy experiments. On one hand, the STM feedback restricts the area of application to the study of single molecules or very thin layers of molecules coated onto metal or other conductive substrates. On the other hand, a metal tip in close proximity to sample molecules on a metal surface is the ideal arrangement for gap-mode TERS experiments, and so far, the only TERS experiments with single-molecule sensitivity have been realized in gap-mode STM-TERS configurations [30-32].

In general, tip fabrication for TEF and TERS is still far from being commercialized. Almost every group working in this field has its own recipe for metallizing commercial AFM tips or fabricating full-metal tips for STM-TERS. Reproducibility is still a big issue, since not every tip shows enhancement and the enhancement factors vary significantly from tip to tip. Also the lifetime of the tip has to be mentioned. In the research labs, the tips are used most often directly after fabrication and last for approximately one day. Since in most cases silver is used, the oxidation of the metal at ambient conditions is the main reason for the loss of enhancement after this time. Additionally, contamination of the tip and generation of strongly Raman scattering amorphous carbon on the metal surface reduce the lifetime of the tips, and in general, SPM tips can be damaged due to mechanical impact and the metal layer can peel off from AFM tips during scanning. Due to these reasons, TEF and TERS are still far from being methods for routine chemical analysis of surfaces. The research in these fields follows a two-pronged approach. On one hand, technical aspects are improved for example to increase sensitivity (down to the single-molecule level) and reproducibility of the tip enhancement. On the other hand, applications in materials science, chemistry, and biology demonstrate the high potential of TEF and TERS to study samples with both, high spatial resolution and chemical contrast.

6. Applications

This section gives examples of applications of TEF and TERS in chemistry, biology, and materials science and summarizes some recent technological improvements of TERS.

6.1 TEF applications

As mentioned above, the first experimental proof for tip-enhanced spectroscopy was a two-photon fluorescence experiment published by E.J. SANCHEZ, L. NOVOTNY, and X.S. XIE in 1999 [24]. They used a gold tip that was prepared by etching and FIB milling and kept at nanometer distances from J aggregates on a glass substrate by a tuning-fork feedback. J aggregates are thin tubular structures formed by self-assembly of certain dye molecules, in this case pseudoisocyanate dye. In order to increase the contrast, two-photon excitation of the dye's fluorescence was performed. Contrary to 'normal' one-photon fluorescence, when using two-photon excitation, the signal intensity depends on the square of the excitation intensity. Thus, the tip-enhanced two-photon fluorescence signal depends on the square of the enhancement factor given by equation (5). Figure 8 shows a topography image and the corresponding TEF image of the J aggregates.

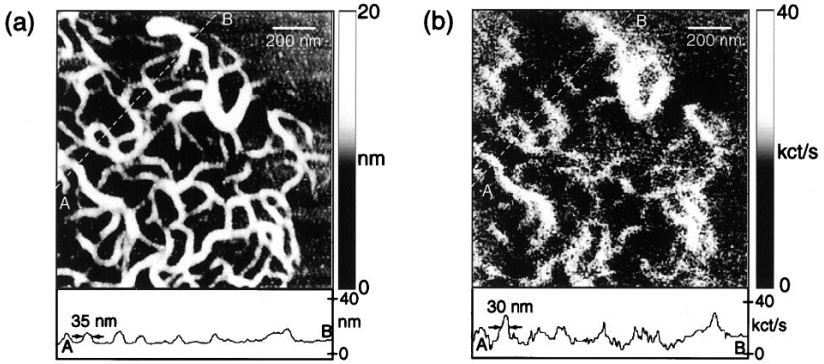

Figure 8: Topography (a) and tip-enhanced two-photon fluorescence images (b) of J aggregates formed by pseudoisocyanate dye. The lower portion of the figure shows cross-sections taken between A and B. Reprinted from Ref. [24], Copyright 1999, with permission from the American Physical Society.

As can be seen, tip-enhanced spectroscopy allows the simultaneous collection of images with complementary information: topography and spectroscopic images can be collected on the exactly same part of a sample. In this point, tip-enhanced spectroscopy definitively overcomes aperture SNOM. Because of their large physical size as compared to AFM or STM tips, the ability of aperture SNOM probes for topography measurements is limited. The cross-sections in Figure 8 highlighting a feature that appears with a width of

35 nm in the topography image demonstrate that the spatial resolution of tip-enhanced spectroscopy (30 nm in this case) can be even better than the resolution of the corresponding topography image. TERS images of carbon nanotubes reveal the same effect [41]. The enhanced electromagnetic field covers most probably only a fraction of the area of the tip apex. Thus, the tip radius, which can be determined by SEM, only gives a rough estimation for the lateral resolution. The TEF or TERS resolution can be significantly smaller than the size of the tip apex. The authors also demonstrate simultaneous topographic and TEF imaging of photosynthetic membrane fragments.

Studying cell membranes with high spatial resolution and chemical contrast is surely one of the most exciting potential fields of application for TEF and TERS and recently, a few groups worldwide have started projects in this area. The group of L. NOVOTNY recently has published images of human erythrocyte membranes revealing the distribution of single Ca^{2+} transmembrane protein channels [42]. The images were collected using a TEF inverted microscope setup and a gold nanoparticle attached to a tip in tuning-fork feedback as a nanoantenna probe. The measurements were performed with the sample immersed in water, which is an important step towards studying cells in their native state. As mentioned already in section 1, one of the drawbacks of fluorescence microscopy is the necessity to stain the sample prior to investigation. In this case, mouse monoclonal antibodies against certain Ca^{2+} transmembrane protein channels were used for tagging the target molecules. Subsequently, anti-mouse antibodies with a fluorescence label were applied for fluorescence staining. Effects of these relatively large molecular labels on the dynamics of the cell membrane will have to be considered, once this technique is applied to living cells. Nevertheless, the results obtained on fixated cell membranes in a liquid environment are very promising. The distribution of the labeled transmembrane proteins, which cannot be investigated by diffraction-limited confocal microscopy, was mapped out with a spatial resolution of approximately 50 nm and an average protein–protein distance of 90 nm has been determined.

6.2 Recent technological improvements of TERS

Recently, our group has published some technical improvements of TERS, which we think will help developing TERS towards a technique for nanoscale chemical analysis of various sample surfaces. As mentioned above, one big issue in TERS is still the poor reproducibility of the tip enhancement. Tips are often produced by vapor coating of AFM tips or electrochemical etching of noble metal wires. Both processes cannot be controlled at the nanometer scale. Thus, there are variations in the geometry of the tip apex visible, when a batch of tips is investigated by SEM. This causes variations of lateral resolution and predominantly of enhancement factors. Even tips that appear very similar in SEM images often show very different enhancement factors, most likely because tip enhancement can be affected by structural differences that are too small to be observed in SEM. Strong signal enhancement can generally be observed when the wavelength of the incident laser has significant overlap with the surface plasmon resonance spectrum of the tip. There are principally two ways to achieve this: (1) tune the laser wavelength and (2) tune the resonance spectrum of the tip. Option (1) is not really feasible due to the lack of continuous-

wave lasers that are tunable over a wide range of the visible spectrum and due to the fact that also the optics, including notch or edge filters, would have to be tuned to different wavelengths. Our group has demonstrated successfully that strategy (2) can improve the signal enhancement in TERS [43-45].

For AFM-TERS, most often commercially available silicon tips are metallized by the user. Silicon tips are cost efficient and widely available in various shapes and with cantilevers covering a wide range of force constants. The surface plasmon resonances of silver nanoparticles have been shown to red shift, when they are attached to materials with high refractive index [46]. Silicon has a relatively high refractive index of $n = 4.4$ causing the surface plasmon resonance of the enhancing silver layer to shift to higher wavelengths. This is unfavorable since in AFM-TERS often lasers with low wavelengths in the visible range (blue to green) are employed for excitation. This is mainly to avoid 'cross-talk' between the TERS laser and the AFM laser (red laser in standard AFMs) that is focused onto the backside of the cantilever for generating the feedback signal for tip–sample distance control. Thus, there is often very weak overlap between laser excitation and surface plasmon resonance of AFM-TERS tips. When tip materials with lower refractive index, such as silicon nitride ($n = 2.05$) or SiO_2 ($n = 1.5$) where used with 488-nm excitation, we obtained significantly higher enhancement factors as compared to the standard silicon tips [45]. This is in good agreement with results from the literature. By comparing enhancement factors obtained by different labs, they were found to be three orders of magnitude higher in the case of a Ag-coated silica fiber tip as compared to metallized silicon AFM probes. Since there are only a few versions of SiO_2 AFM tips on the market and they are much more costly than standard tips made out of silicon or silicon nitride, we developed a two-layer coating method that can be applied to every kind of AFM tip [44]. Here, a dielectric material with low refractive index is coated onto the tip (usually 20–30 nm nominal thickness) followed by a Ag layer (20–30 nm). Low-refractive index materials used by our group are silicon oxide (SiO_x, $n = 1.5$–2.05, depending on x) and aluminum fluoride ($n = 1.4$). They can be coated onto the tips by sublimation of the substance in a vacuum coating chamber by resistive heating. Both materials covered with a Ag layer have yielded strong enhancement of Raman signals with 488-nm excitation. The highest enhancement factor of approx. 4–5×10^4 was achieved with AlF_3-Ag coating and brillant cresyl blue (BCB) dye coated onto a glass substrate as a sample. Contrasts obtained were on the order of 70–80. The results were confirmed by SERS measurements [44]. Also there, pre-coating of the substrates with low-refractive index materials has significantly improved the enhancement. The explanation of the stronger enhancement based on the shifted surface plasmon resonance spectrum was confirmed by numerical simulation of the spectra by a finite element method [43].

We also studied the effect of the angle in which the tip is approached to the sample surface [45]. The angle affects the orientation of the tip axis with respect to the polarization direction of the incoming light. Additionally, the tip touches the surface with a different part of its apex, when the whole AFM head is tilted by a certain angle. We found, that by changing the angle of the AFM head with respect to the sample surface, tips which did not show any enhancement before, appeared to be 'hot' when approached in a different angle. It seems that non-enhancing tips often just do not touch the sample with a 'hot' site. By

combining the two-layer coating with the variable-angle approach, almost every tip showed TERS enhancement. Since there are still very significant variations of the enhancement factor from tip to tip, there is still room for improvements.

Performing measurements in liquids is very important, when cells are studied in their native environment. There have been mainly two issues to be solved for operating a TERS experiment with the sample surface and tip totally immersed in water. First, the tip has to provide reasonable enhancement and stability in water and second, the tip has to be protected from being contaminated by molecules dissolved in the liquid environment. Experiments by our group have demonstrated that AFM tips coated with SiO_x and Ag by the two-layer method can reasonably enhance Raman signals and are mechanically stable in water [47]. Other tip coatings, such as AlF_3-Ag, peel off the tip surface when the TERS probe is immersed in water. The second issue was contamination of the tip by sample molecules that have been desorbed from the surface and transported to the tip through the aqueous phase. Extensive contamination of the tip surface is usually the end of a TERS experiment, because the same spectrum is observed throughout the whole experiment, independently of the tip position on the sample. Furthermore, contaminants on the silver surface can easily be degraded into amorphous carbon under laser irradiation. Amorphous carbon is a strong Raman scatterer and its spectrum easily overwhelms the spectra of analyte molecules. In TERS experiments in water, the tips have successfully been protected from contaminations by coating them with a self-assembled monolayer (SAM) of ethane thiol. This molecule binds strongly to silver and prevents adsorbtion of contaminations to the silver surface. Furthermore, only one relatively strong Raman band of ethane thiol was observed, which did not affect the evaluation of analyte bands. We think that this proof-of-principle study of TERS in liquids can pave the way for studying unlabeled cell membranes in their native environment with high spatial resolution and chemical contrast.

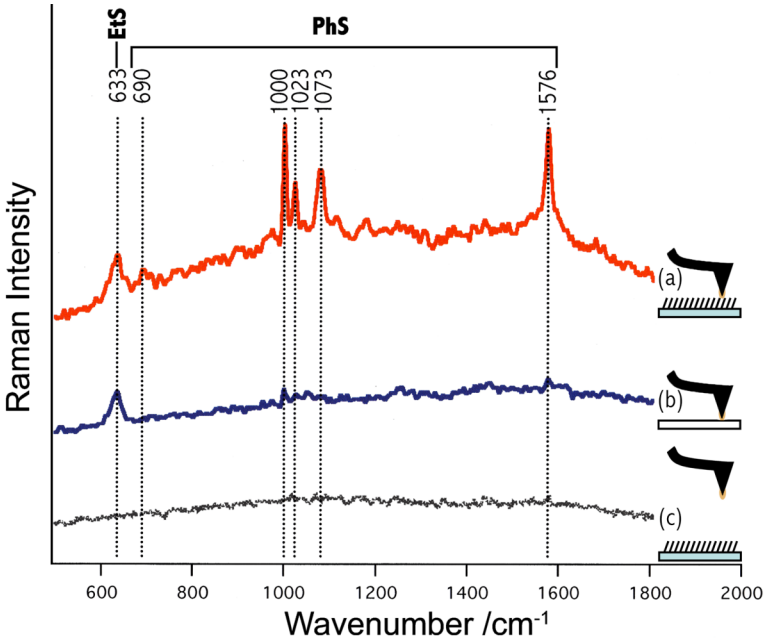

Figure 9: TERS experiment performed in water using a SiO_x-Ag-coated AFM tip covered with an ethane thiol (EtS) protection layer: tip in contact with a thiophenol (PhS) layer on a gold substrate (a), tip in contact with a clean glass slide after measurement (a) for control of possible tip contamination (b), and far field spectrum collected with the tip far away from the sample surface (c). Adapted from Ref. [47].

As mentioned in section 5, there have been basically two possibilities to study opaque samples with TERS (see Figure 6, side-illumination and parabolic-mirror setup). Approaches based on side-illumination have the drawback of lowered focus quality and reduced collection efficiency due to the use of low-*NA* long-working distance objectives in an off-axis configuration. Highly symmetric and tightly focused illumination of the tip as well as highly efficient collection can be achieved by parabolic-mirror approaches, but these are difficult to align and slight changes of the alignment dramatically affect focusing and collection. Both, side-illumination and parabolic-mirror approach, cannot be combined with a laser-scanning microscope. The laser-scanning microscope often used in inverted microscope setups is very advantageous for TERS. Scanning the laser while collecting confocal images or Raman spectra allows imaging of the tip and sample followed by precise positioning of the laser spot on the 'hot' site of the tip. Afterwards the sample is scanned while keeping the laser–tip alignment fixed, and enhanced Raman scattering at a selected wavenumber or full TER spectra are collected at every pixel of the sample. Contrarily, when using side-illumination approaches, the laser–tip alignment often has to be performed manually by checking the intensity of scattered light 'by eye'. This results in less precise

alignment and needs very experienced users. Recently, we were able to overcome these problems by using combinations of an upright microscope with STM [48] and AFM [49]. A relatively large objective offering high NA and long working distance at the same time and electrochemically etched STM or specially shaped, vapor-coated AFM tips enabled the collection of TER spectra with illumination and collection performed exactly from top. The upright microscope for opaque samples is equipped with laser and sample scanning modules and thus, offers the same functionality as an inverted microscope setup. We expect, this will open the field of opaque real-world samples, such as nanostructured materials, for investigation by TERS. Results and technical details of this novel TERS setup will be published elsewhere.

6.3 TERS applications

TERS experiments have been performed with a large variety of samples. This section only gives a few selected examples. Thin films down to sub-monolayers of dye molecules are often the 'standard' samples for TERS. Often due to resonance enhancement, they provide relatively strong Raman scattering allowing the collection of both, the enhanced near-field and non-enhanced far-field signals and determination of enhancement factors. Both, the first TERS [25, 27] and the first single-molecule TERS experiments [30-32] published in literature where based on dye molecules.

Single-walled carbon nanotubes (SWNT) are formed in various diameters, and can have different chiralities and structures leading to insulating, semiconducting or metallic properties. These features can be studied by Raman spectroscopy. TERS allows the collection of spectra on different spots of a single carbon nanotube and reveals structural heterogeneities inside a single nanotube [37, 50]. In this way, changes in diameter or between semiconducting and metallic properties have been found. Measurements of carbon nanotubes also revealed that the resolution of TERS is in some cases better than the topographic resolution obtained with the same tip [41]. The same effect has been observed in TEF experiments (see section 6.1, Figure 8) indicating that the enhanced field covers only a fraction of the tip apex [24]. Another inorganic material that has been analyzed by TERS is silicon [51-53]. Stress mapping of silicon semiconductors with nanometer-scale resolution is gaining importance because of the ongoing miniaturization of semiconductor circuits. TERS allows the detection of stress-induced band shifts of the most prominent silicon band at approx. 520 cm^{-1} with high spatial resolution. Indeed, the use of alternative AFM tip materials or full-metal tips is preferred in this field of application because the Raman signals of silicon AFM tips would interfere with the sample signals.

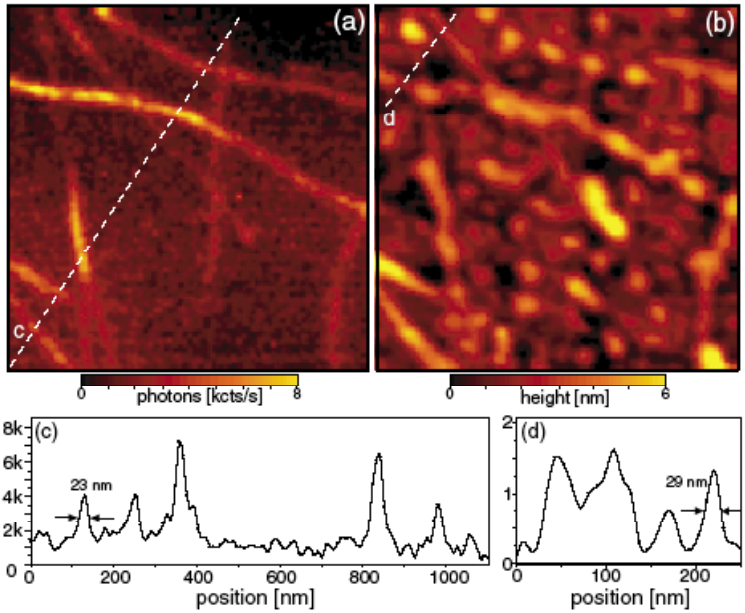

Figure 10: TERS image (a) and topographic image (b) of single-walled carbon nanotubes on a glass substrate, and cross sections along the dashed lines in the images (c, d) Reprinted from Ref. [37], Copyright 2003, with permission from the American Physical Society.

Investigating biological samples by TERS is surely very exciting, because TERS offers topographic and chemical information with a spatial resolution that is one order of magnitude better than in conventional confocal microscopy. Since TERS is a surface-sensitive technique, the inside of a cell would only be accessible to TERS in the form of microtome cuts. On the other hand, surface-sensitivity is advantageous, when for example only the surface of a cell should be studied. We think that studying cell membranes with high spatial resolution and chemical contrast will provide deeper insight in many biological processes and solve open questions, such as the existence and size of lipid rafts. Cell membranes consist of a complex mixture of lipids, proteins and sugars. They are involved in many fundamental biological processes, such as enzymatic reactions, exchange of ions and molecules between the cytosol and the extracellular space, cell–cell signaling, and are linked to various diseases. Lipid rafts are thought to be aggregates of certain sphingolipids and cholesterol with a size of < 200 nm, which can self-assemble in the membrane and influence the arrangement of membrane proteins [54]. Existence and size of lipid rafts is still under debate, because until now no experiment was able to directly image such aggregates. We expect tip-enhanced spectroscopy to yield important information in this field. Since antibody labels could probably affect the dynamics of the cell membrane, the use of the label-free

TERS technique is advantageous compared to TEF. Full-spectroscopic imaging of cell surfaces can map out the distribution of many different compounds at the same time. This is a prerequisite for a better understanding of such complex biological systems. A few groups worldwide have started activities in this field. J. POPP, V. DECKERT, and co-workers have published first results of TERS measurements on lipid layers [55]. TERS measurements of complex biological systems in general show that assignment of Raman bands in the relatively complex spectra to certain compounds is very difficult. Thus, in the lipid TERS project of our group, measurements of lipid layers and cell membranes as well as normal Raman, SERS and TERS measurements of pure biomolecules are performed. The latter have the goal of building up a spectral database, which in future should allow much more precise band assignments.

In general, TERS measurements of pure biomolecules are an important step towards the investigation of more complex biological systems. Due to selection rules and chemical enhancement effects, TERS spectra of complex molecules can significantly differ from normal Raman spectra. TERS measurements of biomolecules can help understanding these effects and yield reference spectra for measurements of complex biological matrices. The group of S. KAWATA investigated the distribution of DNA molecules on surfaces based on tip-enhanced coherent anti-Stokes Raman scattering (CARS) [56]. They also found that the TER spectrum of adenine significantly varies due to chemical enhancement effects, depending on which of the nitrogen atoms binds to the silver surface [57]. Specific chemical enhancement of the protein backbone enabled our group to excite Raman bands of the apoprotein of cytochrome c [58]. The protein bands in normal Raman and SERS spectra of this protein collected in the visible spectral range are overwhelmed by the resonantly enhanced heme bands. Only TERS allows to study amino acid and heme bands simultaneously. Also the TER spectrum of the polysaccharide alginate differs significantly from the normal Raman spectrum [59]. Chemical enhancement effects cause band shifts, which are also observed in SERS spectra of this compound. Alginate is an important stabilizing compound found in the extracellular matrix of bacterial biofilms.

Biofilms are another example for biological surfaces, where nanoscale chemical analysis by TERS can provide deeper insight. Biofilms are the predominant life-form of bacteria, which can colonize almost every solid surface. They are of high importance in biology, medicine, ecology, wastewater treatment, and other technological processes. Apart from the cell surfaces, the extracellular matrix is an interesting target for TERS investigation. It is formed by a complex mixture of biopolymers that are excreted by the bacteria and form a stable and protecting environment for bacteria. Thus, composition of the matrix and spatial arrangement of the different polymers as well as their interactions with the cells have a direct effect on function and stability of the biofilm. As shown by our group, combined AFM–Raman investigations allow the determination of important properties of biofilms, such as size and arrangement of extracellular structures [60], distribution of cyanobacteria inside biofilms [61], and crystal structure of microbially generated mineral nanoparticles, such as dolomite [62]. We expect that TERS will provide deeper insight in the spatial distribution of various compounds inside the highly heterogeneous biofilm matrix.

7. Conclusions

Tip-enhanced spectroscopies provide chemical analysis of sample surfaces with a lateral resolution of 10–50 nm. Tip-enhancement is often a combination of different enhancement effects, such as lightning rod effect, localized surface plasmon resonances, antenna enhancement, and chemical enhancement effects. The tips used are most often metal-coated AFM probes or electrochemically etched full-metal tips in STM or shear-force feedback. The tips are laser-illuminated and optical signals are collected using inverted microscope setups for transparent samples, or side-illumination or parabolic-mirror setups for opaque samples. Tip-enhanced spectroscopy overcomes drawbacks of aperture SNOM, most importantly the limited throughput of glass fiber tips and the limited quality of topography images collected with the relatively large aperture SNOM probes.

Tip-enhanced fluorescence (TEF) often needs staining of the sample before analysis, because only fluorophores are visible in a TEF image. This makes data interpretation relatively simple, but leads also to several drawbacks. For example, the fluorescence label could affect the sample and cause artifacts, for every analyte molecule there has to be an appropriate fluorescence label available, and the presence of a molecule in the sample has to be known in advance. Furthermore, for practical reasons only a very limited number of different molecules can be investigated simultaneously. These drawbacks can be overcome by using the label-free technique of tip-enhanced Raman spectroscopy (TERS). TERS provides molecular fingerprints of the sample with nanometer-scale spatial resolution. The sharp Raman bands allow mapping the distribution of a large number of different molecules simultaneously. TEF and TERS are still far from being techniques for routine chemical analysis, but recent technological developments are surely important steps in this direction by improving the tip enhancement and its reproducibility, enabling measurements in liquid environments, and extending the possibilities to study opaque samples.

TEF and TERS have been applied to a wide range of samples from chemistry, biology, and materials science. Examples of studies of dye molecules, carbon nanotubes, and silicon have been briefly discussed. Studying biological surfaces with high spatial resolution and chemical contrast will provide deeper insight in many important biological processes. Cell membranes are a good example for biological surfaces that are involved in many important processes and are highly heterogeneous at the nanometer scale. For a correct assignment of bands in the complex spectra of biological systems, reference measurements of pure biomolecules have to be performed. Examples of measurements of nucleic acids, proteins, and polysaccharides have been mentioned in section 6.3 of this contribution. Bacterial biofilms, especially the highly complex extracellular matrix, are another interesting target for nanoscale chemical analysis, and we expect that TERS will yield important information on the structure of biofilms and other biological samples in future.

References

1. E. Abbe, Beitraege zur Theorie des Mikroskops und der mikroskopischen Wahrnehmung, *Arch. mikrosk. Anat. Entwichlungsmech.* **9** (1873), 413-468.

2. L. Rayleigh, Investigations in Optics, with Special Reference to the Spectroscope, *Philos. Mag.* **8** (1879), 261-274.
3. E. H. Synge, A Suggested Method for Extending Microscopic Resolution into the Ultra-Microscopic Region, *Philos. Mag.* **6** (1928), 356-362.
4. E. A. Ash and G. Nicholls, Super-resolution Aperture Scanning Microscope, *Nature* **237** (1972), 510-512.
5. G. Binnig, H. Rohrer, C. Gerber and E. Weibel, Surface Studies by Scanning Tunneling Microscopy, *Phys. Rev. Lett.* **49** (1982), 57-61.
6. D. W. Pohl, W. Denk and M. Lanz, Optical Stethoscopy - Image Recording with Resolution Lambda/20, *Appl. Phys. Lett.* **44** (1984), 651-653.
7. A. Lewis, M. Isaacson, A. Hrootunian and A. Muray, Development of a 500 Å Spatial Resolution Light Microscope: I. Light is Efficiently Transmitted Through Lambda/16 Diameter Apertures, *Ultramicrosc.* **13** (1984), 227-231.
8. R. C. Dunn, Near-Field Scanning Optical Microscopy, *Chem. Rev.* **99** (1999), 2891-2927.
9. D. P. Tsai, A. Othonos, M. Moskovits and D. Uttamchandani, Raman Spectroscopy Using a Fiber Optic Probe with Subwavelength Aperture, *Appl. Phys. Lett.* **64** (1994), 1768-1770.
10. D. A. Smith, S. Webster, M. Ayad, S. D. Evands, D. Fogherty and D. Batchelder, Development of a Scanning Near-Field Optical Probe for Localized Raman Spectroscopy, *Ultramicrosc.* **61** (1995), 247-252.
11. S. Webster, D. N. Batchelder and D. A. Smith, Submicron Resolution Measurement of Stress in Silicon by Near-Field Raman Spectroscopy, *Appl. Phys. Lett.* **72** (1998), 1478-1480.
12. C. L. Jahncke, M. A. Paesler and H. D. Hallen, Raman Imaging with Near-Field Scanning Optical Microscopy, *Appl. Phys. Lett.* **67** (1995), 2483-2485.
13. C. L. Jahncke, H. D. Hallen and M. A. Paesler, Nano-Raman Spectroscopy and Imaging with a Near-Field Scanning Optical Microscope, *J. Raman Spectrosc.* **27** (1996), 579-586.
14. R. Stöckle, C. Fokas, V. Deckert, R. Zenobi, B. Sick, B. Hecht and U. P. Wild, High-Quality Near-Field Optical Probes by Tube Etching, *Appl. Phys. Lett.* **75** (1999), 160-162.
15. D. Zeisel, V. Deckert, R. Zenobi and T. Vo-Dinh, Near-Field Surface-Enhanced Raman Spectroscopy of Dye Molecules Adsorbed on Silver Island Films, *Chem. Phys. Lett.* **283** (1998), 381-385.
16. R. Zenobi and V. Deckert, Scanning near-field optical microscopy and spectroscopy as a tool for chemical analysis, *Angew. Chem.-Int. Ed.* **39** (2000), 1746-1756.
17. J. Wessel, Surface-Enhanced Optical Microscopy, *J. Opt. Soc. Am. B* **2** (1985), 1538-1541.
18. L. Novotny, The History of Near-field Optics, *Prog. Optics* **50** (2007), 137-184.
19. F. Keilmann and R. Hillenbrand, Near-Field Microscopy by Elastic Light Scattering from a Tip, *Phil. Trans. Royal Soc. London Series A - Math. Phys. Eng. Sci.* **362** (2004), 787-805.
20. A. J. Huber, D. Kazantsev, F. Keilmann, J. Wittborn and R. Hillenbrand, Simultaneous IR Material Recognition and Conductivity Mapping by Nanoscale Near-Field Microscopy, *Adv. Mater.* **19** (2007), 2209-2212.
21. T. Taubner, R. Hillenbrand and F. Keilmann, Nanoscale Polymer Recognition by Spectral Signature in Scattering Infrared Near-Field Microscopy, *Appl. Phys. Lett.* **85** (2004), 5064-5066.
22. R. Hillenbrand and F. Keilmann, Material-Specific Mapping of Metal/Semiconductor/Dielectric Nanosystems at 10 nm Resolution by Backscattering Near-Field Optical Microscopy, *Appl. Phys. Lett.* **80** (2002), 25-27.

23. U. C. Fischer and D. W. Pohl, Observation of Single-Particle Plasmons by Near-Field Optical Microscopy, *Phys. Rev. Lett.* **62** (1989), 458-461.

24. E. J. Sanchez, L. Novotny and X. S. Xie, Near-Field Fluorescence Microscopy Based on Two-Photon Excitation With Metal Tips, *Phys. Rev. Lett.* **82** (1999), 4014-4017.

25. R. M. Stöckle, Y. D. Suh, V. Deckert and R. Zenobi, Nanoscale Chemical Analysis by Tip-Enhanced Raman Spectroscopy, *Chem. Phys. Lett.* **318** (2000), 131-136.

26. M. S. Anderson, Locally Enhanced Raman Spectroscopy with an Atomic Force Microscope, *Appl. Phys. Lett.* **76** (2000), 3130-3132.

27. N. Hayazawa, Y. Inouye, Z. Sekkat and S. Kawata, Metallized Tip Amplification of Near-Field Raman Scattering, *Opt. Commun.* **183** (2000), 333-336.

28. A. Hartschuh, Tip-Enhanced Near-Field Optical Microscopy, *Angew. Chem.-Int. Ed.* **47** (2008), 2-18.

29. B. Pettinger, G. Picardi, R. Schuster and G. Ertl, Surface-Enhanced and STM-Tip-Enhanced Raman Spectroscopy at Metal Surfaces, *Single Mol.* **3** (2002), 285-294.

30. C. C. Neacsu, J. Dreyer, N. Behr and M. B. Raschke, Scanning-probe Raman spectroscopy with single-molecule sensitivity, *Phys. Rev. B* **73** (2006), 193406.

31. W. Zhang, B. S. Yeo, T. Schmid and R. Zenobi, Single Molecule Tip-Enhanced Raman Spectroscopy with Silver Tips, *J. Phys. Chem. C* **111** (2007), 1733-1738.

32. J. Steidtner and B. Pettinger, Tip-Enhanced Raman Spectroscopy and Microscopy on Single Dye Molecules with 15 nm Resolution, *Phys. Rev. Lett.* **100** (2008), 236101.

33. I. Nothinger and A. Elfick, Effect of Sample and Substrate Electric Properties on the Electric Field Enhancement at the Apex of SPM Nanotips, *J. Phys. Chem. B* **109** (2005), 15699-15706.

34. T. Schmid, B. S. Yeo, W. Zhang and R. Zenobi, Use of Tip-Enhanced Vibrational Spectroscopy for Analytical Applications in Chemistry, Biology and Materials Science, in: S. Kawata and V. M. Shalaev (eds.), *Tip Enhancement: Advances in Nano-Optics and Nano-Photonics*, Elsevier B.V., Amsterdam, 2007.

35. F. M. Huang and D. Richards, Fluorescence Enhancement and Energy Transfer in Apertureless Scanning Near-Field Optical Microscopy, *J. Opt. A-Pure Appl. Op.* **8** (2006), S234-S238.

36. P. Anger, P. Bharadwaj and L. Novotny, Enhancement and Quenching of Single-Molecule Fluorescence, *Phys. Rev. Lett.* **96** (2006), 113002.

37. A. Hartschuh, E. J. Sanchez, X. S. Xie and L. Novotny, High-Resolution Near-Field Raman Microscopy of Single-Walled Carbon Nanotubes, *Phys. Rev. Lett.* **90** (2003), 095503.

38. W. Zhang, H. Fischer, T. Schmid, R. Zenobi and O. J. F. Martin, Mode-Selective Surface-Enhanced Raman Spectroscopy Using Nanofabricated Plasmonic Dipole Antennas, *J. Phys. Chem. C* **113** (2009), 14672-14675.

39. T. Schmid, B. S. Yeo, W. Zhang and R. Zenobi, Spectroscopic Imaging with Nanometer Resolution Using Near-Field Methods, in: R. Salzer and H. W. Siesler (eds.), *Infrared and Raman Spectroscopic Imaging*, Wiley-VCH, Weinheim, 2009.

40. J. Stadler, C. Stanciu, C. Stupperich and A. J. Meixner, Tighter Focusing with a Parabolic Mirror, *Opt. Lett.* **33** (2008), 681-683.

41. A. Hartschuh, N. Anderson and L. Novotny, Near-Field Raman Spectroscopy Using a Sharp Metal Tip, *J. Microsc.-Oxford* **210** (2003), 234-240.

42. C. Hoppener and L. Novotny, Antenna-Based Optical Imaging of Single Ca2+ Transmembrane Proteins in Liquids, *Nano Lett.* **8** (2008), 642-646.

43. X. D. Cui, W. H. Zhang, B. S. Yeo, R. Zenobi, C. Hafner and D. Erni, Tuning the resonance frequency of Ag-coated dielectric tips, *Optics Express* **15** (2007), 8309-8316.

44. B. S. Yeo, T. Schmid, W. Zhang and R. Zenobi, Towards Rapid Nanoscale Chemical Analysis using Tip-Enhanced Raman Spectroscopy with Ag-Coated Dielectric Tips, *Anal. Bioanal. Chem.* **387** (2007), 2655-2662.

45. B. S. Yeo, W. Zhang, C. Vannier and R. Zenobi, Enhancement of Raman Signals with Silver-Coated Tips, *Appl. Spectrosc.* **60** (2006), 1142-1147.

46. K. L. Kelly, E. Coronado, L. L. Zhao and G. C. Schatz, The Optical Properties of Metal Nanoparticles: The Influence of Size, Shape, and Dielectric Environment, *J. Phys. Chem. B* **107** (2003), 668-677.

47. T. Schmid, B. S. Yeo, G. Leong, J. Stadler and R. Zenobi, Performing Tip-Enhanced Raman Spectroscopy in Liquids, *J. Raman Spectrosc.* **40** (2009), 1392-1399.

48. J. Stadler, T. Schmid and R. Zenobi, experimental details and results will be published elsewhere.

49. T. Schmid, J. Stadler, L. Opilik, R. M. Balabin and R. Zenobi, experimental details and results will be published elsewhere.

50. N. Anderson, A. Hartschuh and L. Novotny, Chirality changes in carbon nanotubes studied with near-field Raman spectroscopy, *Nano Lett.* **7** (2007), 577-582.

51. V. Poborchii, T. Tada and T. Kanayama, Subwavelength-resolution Raman microscopy of si structures using metal-particle-topped AFM probe, *Jpn. J. Appl. Phys. Part 2 - Lett. Express Lett.* **44** (2005), L202-L204.

52. W. X. Sun and Z. X. Shen, Near-field scanning Raman microscopy using apertureless probes, *J. Raman Spectrosc.* **34** (2003), 668-676.

53. W. X. Sun and Z. X. Shen, Apertureless near-field scanning Raman microscopy using reflection scattering geometry, *Ultramicrosc.* **94** (2003), 237-244.

54. L. J. Pike, The Challenge of Lipid Rafts, *J. Lipid Res.* **50** (2009), S323-S328.

55. R. Boehme, M. Richer, D. Cialla, P. Roesch, V. Deckert and J. Popp, Towards a Specific Characterisation of Components on a Cell Surface – Combined TERS-Investigations of Lipids and Human Cells, *J. Raman Spectrosc.* **40** (2009), 1452-1457.

56. T. Ichimura, N. Hayazawa, M. Hashimoto, Y. Inouye and S. Kawata, Tip-enhanced coherent anti-Stokes Raman scattering for vibrational nanoimaging, *Phys. Rev. Lett.* **92** (2004),

57. H. Watanabe, Y. Ishida, N. Hayazawa, Y. Inouye and S. Kawata, Tip-enhanced near-field Raman analysis of tip-pressurized adenine molecule, *Phys. Rev. B* **69** (2004), 155418.

58. B. S. Yeo, S. Madler, T. Schmid, W. H. Zhang and R. Zenobi, Tip-Enhanced Raman Spectroscopy Can See More: The Case of Cytochrome C, *J. Phys. Chem. C* **112** (2008), 4867-4873.

59. T. Schmid, A. Messmer, B. S. Yeo, W. H. Zhang and R. Zenobi, Towards Chemical Analysis of Nanostructures in Biofilms II: Tip-Enhanced Raman Spectroscopy of Alginates, *Anal. Bioanal. Chem.* **391** (2008), 1907-1916.

60. T. Schmid, J. Burkhard, B. S. Yeo, W. H. Zhang and R. Zenobi, Towards Chemical Analysis of Nanostructures in Biofilms I: Imaging of Biological Nanostructures, *Anal. Bioanal. Chem.* **391** (2008), 1899-1905.

61. T. Schmid, A. Sebesta, J. Stadler, L. Opilik, R. M. Balabin and R. Zenobi, Tip-Enhanced Raman Spectroscopy and Related Techniques in Studies of Biological Materials, *Proc. SPIE* **7586** (2010), 758603.

62. M. Sánchez-Román, C. Vasconcelos, T. Schmid, M. Dittrich, J. A. McKenzie, R. Zenobi and M. A. Rivadeneyra, Aerobic Microbial Dolomite at the Nanometer Scale: Implications for the Geologic Record, *Geology* **36** (2008), 879-882.